

Article

Creep of Heusler-Type Alloy Fe-25Al-25Co

Ferdinand Dobeš¹, Petr Dymáček^{1,2} and Martin Friák^{1,2,*} 

¹ Institute of Physics of Materials, Academy of Sciences of the Czech Republic, Žižkova 22, CZ-61662 Brno, Czech Republic; dobes@ipm.cz (F.D.); pdymacek@ipm.cz (P.D.)

² CEITEC IPM, Institute of Physics of Materials, Academy of Sciences of the Czech Republic, Žižkova 22, CZ-61662 Brno, Czech Republic

* Correspondence: friak@ipm.cz; Tel.: +420-532-290-400

Received: 20 December 2019; Accepted: 16 January 2020; Published: 20 January 2020



Abstract: Creep of an alloy based on the intermetallic compound Fe₂AlCo was studied by compressive creep tests in the temperature range from 873 to 1073 K. The stress exponent n and the activation energy of creep Q were determined using the multivariable regression of the creep-rate data and their description by means of sinh equation (Garofalo equation). The evaluated stress exponents indicate that the dislocation climb controls creep deformation. The estimated apparent activation energies for creep are higher than the activation enthalpy for the diffusion of Fe in Fe₃Al. This can be ascribed to the changes in crystal lattice and changing microstructure of the alloy.

Keywords: iron aluminides; Heusler alloy; creep; stress exponent; activation energy

1. Introduction

Fe–Al-based alloys are potential candidates for new structural materials due to their outstanding corrosion resistance in various hostile environments, relatively low density and the low cost of both the basic constituting elements [1–3]. Insufficient creep resistance has been identified as an obstacle for their extensive application at high temperatures [4,5]. A number of methods have been proposed to overcome this problem. These include solid-solution hardening, strengthening by second-phase particles or ordering [6,7]. A promising method of strengthening is the addition of an element that leads to the formation of the Heusler compound [8,9]. These compounds are currently attracting research attention due to the many interesting properties they possess. In the Fe–Al system, the compound can be formed by the addition of 3d-transition elements: Sc, Ti, V, Cr, Mn, Co, Ni, Cu, and Zn were considered theoretically by Gilleßen and Dronskowski [10]. Among these elements, Co leads to the largest increase of Young’s modulus, and Voigt shear modulus [11]. A very high Curie temperature of 857 °C was also found in the Fe₂CoAl compound [12]. In the previous study, quantum-mechanical calculations were used to investigate properties of four different polymorphs of Fe₂AlCo and the occurrence of structural multiplicity at elevated temperatures was predicted [13]. Very few studies have experimentally investigated mechanical properties of Heusler compounds [14]. As far as we know, only Fe₂AlTi-containing alloys were subjected to mechanical testing at elevated temperatures within the Fe–Al system [15–17]. The present study examines the creep behavior of a Fe₂AlCo-based alloy and describes it in terms of the Garofalo equation [18]. The results are interpreted in terms of the available ternary phase diagrams and compared with the results of testing Fe–Al–Ti alloys.

The Fe₂AlCo has, under 1000 K, a two-phase superalloy nanostructure with cuboids of a partly ordered phase coherently co-existing in a differently (or less) ordered matrix. The ordered phase has not the full-Heusler lattice (the L₂₁ structure as a ternary analogue of D0₃) because quantum-mechanical calculations showed that it is mechanically unstable [13] and the inverse-Heusler structure, cf., Figure 1a, is both mechanically and thermodynamically more stable [10,13]. The inverse-Heusler is also in a better

agreement with experiments (see, e.g., Ref. [19]). In the high-temperature range, the arrangement of atoms may become even less ordered, exhibiting B2 and A2 lattices (Figure 1b,c).

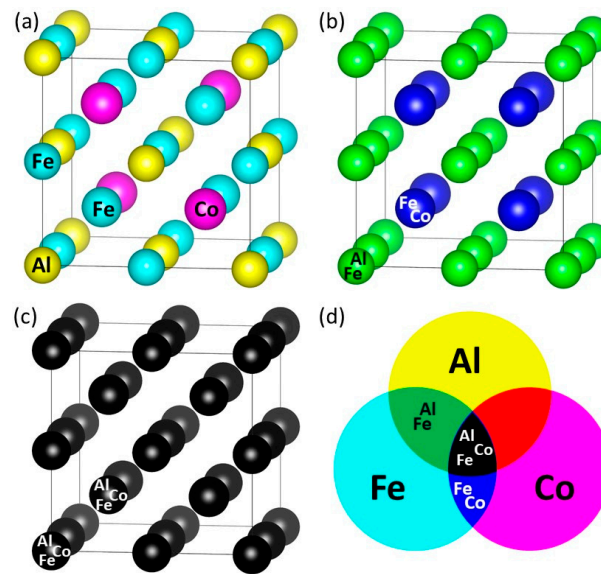


Figure 1. Schematic visualizations of atom configurations in Fe_2AlCo : an inverse-Heusler (a), a partially ordered B2 (b) and a disordered A2 (c). A schematic of the used coloring of atoms (d).

Although the composition of the studied alloy is close to the stoichiometric composition of Heusler alloys, we refer to our alloy as the Heusler-type alloy. In accordance with the more recent phase diagrams (see below), we assume that the A2 and B2 lattices coherently coexist at the nanoscale level (cuboids with the size of dozens of nm embedded in a matrix) at high temperatures.

2. Materials and Methods

The alloy was prepared using vacuum induction melting and casting under argon into a cylindrical cast of diameter 20 mm and exploitable length of 200 mm. The nominal composition of the alloy, 25 at. % Al and 25 at. % Co, is marked in parts of isothermal sections of the ternary Fe–Al–Co diagram in Figure 2 [20]. The grains are large and have an elongated shape with a mean aspect ratio of 4:1; the mean width is approximately 250 μm , see Figure 3.

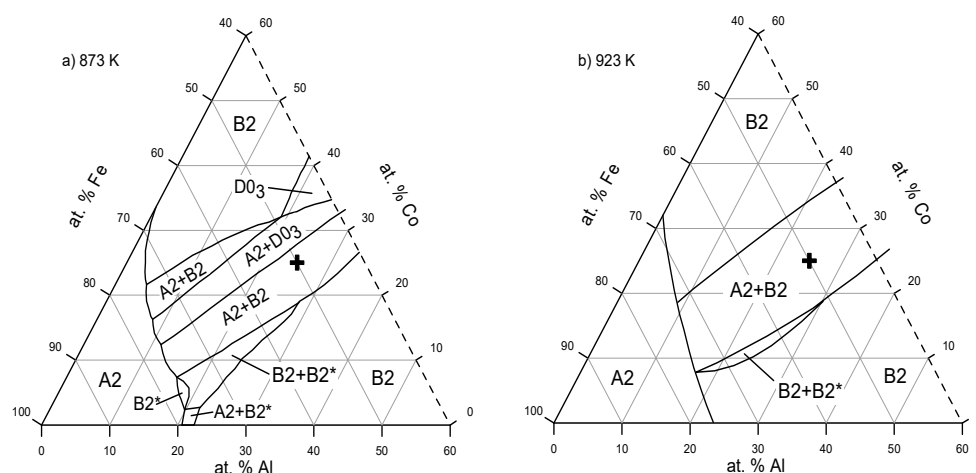


Figure 2. Details of the isothermal sections of the Fe–Al–Co system at (a) 873 K, calculated, and (b) 923 K, experimental, according to Kozakai et al. [20].

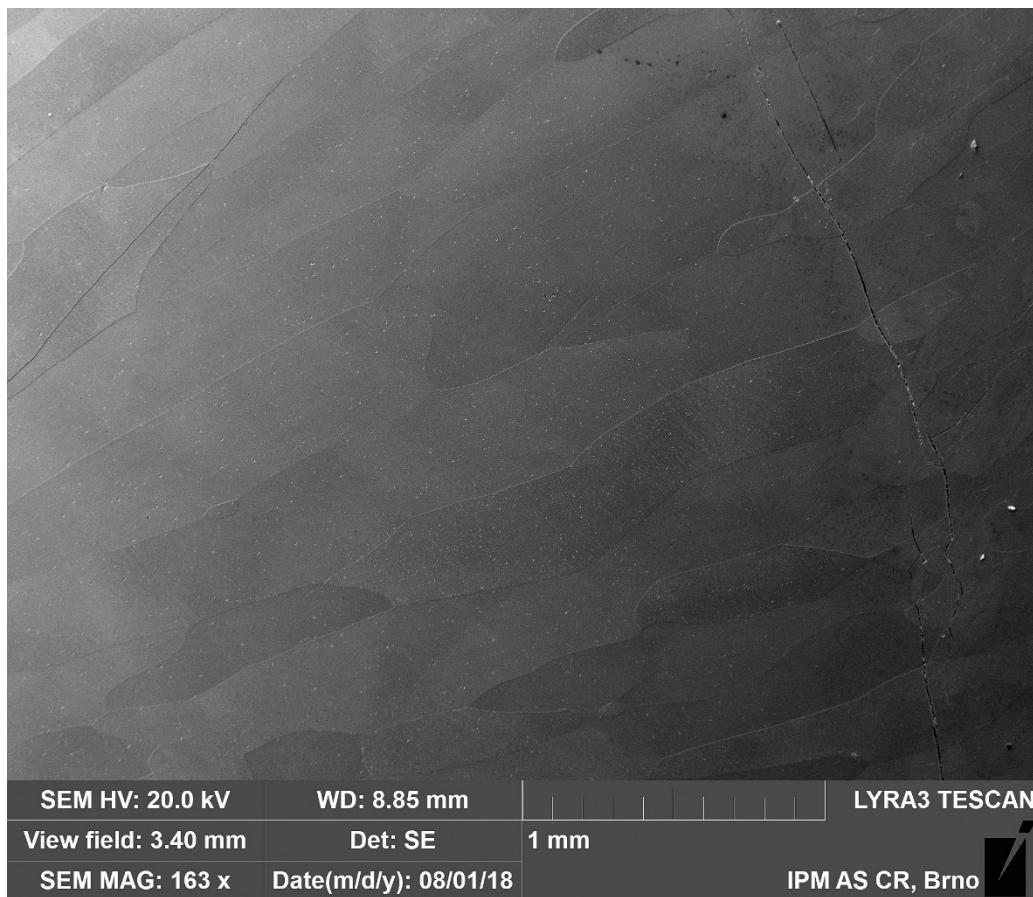


Figure 3. Backscattered electron micrograph of metallographic section of the uncrept alloy.

Creep tests were performed in uniaxial compression on samples with a gauge length of 10 mm and a cross-section of $5 \times 5 \text{ mm}^2$. The compressive testing allows creep deformation not affected by the onset of fracture processes to be studied. On the other hand, because of the need for a specific compressive cage (reversible grips), the test arrangement does not allow rapid cooling of the test specimen, and not even cooling under the effect of load. Effective observation of the microstructure after creep is, therefore, limited. The samples were prepared by travelling wire electro-discharge machining and fine grinding of the surfaces. The tests were performed under a constant load on a dead-weight creep machine that was constructed in-house in a protective atmosphere of dry purified. The test temperature was held constant within $\pm 1 \text{ K}$ for each individual test. Changes in the gauge length were measured using a linear variable displacement transducer. The samples were subjected to stepwise loading, where the load was changed after the steady-state creep rate was established for a given load. The terminal values of the true stress and the creep rate, i.e., the true compressive strain rate, were evaluated for each step.

3. Results

Figure 4 shows the variation of creep rate $\dot{\epsilon}$ with the applied stress σ at different temperatures T in a double-logarithmic plot. From the figure, it is obvious that a simple power law is not able to describe the measured data even in the area of the highest temperatures. The mean value of the power n' is equal to 3.8 at 1073 K and 4.6 at 1023 K, but even at these temperatures, an increase in the power at higher stresses, which is commonly referred to in the literature as a power law breakdown, is observable. A single relation that satisfies conditions for both low and high stresses is the relationship proposed by Garofalo [18,21].

$$\dot{\epsilon} = A'' \sigma^{n'} \quad (1)$$

$$\dot{\epsilon} = A' [\sinh(B\sigma)]^n \quad (2)$$

where A' , B and n are stress-independent parameters. Moreover, the parameter A' is usually temperature dependent and this dependence can be expressed by means of Arrhenius function [22–24]. Equation (2) then reads

$$\dot{\epsilon} = A \exp\left(\frac{-Q}{RT}\right) [\sinh(B\sigma)]^n \quad (3)$$

where Q is the activation energy and R is the universal gas constant. The values of parameters in Equation (3) can be found by multivariable regression of the measured data (Table 1). The analysis was performed separately for high temperatures (1023 K and 1073 K) and low temperatures (873 K, 923 K and 973 K). The resulting values are presented in $\times 1$. It should be noted that the Garofalo equation is an empirical equation based on the evaluation of creep data of single-phase materials: (Cu, Al, Al-3Mg) and austenitic steel. However, it can also be used to describe data of multiphase materials [25]. Its use in describing rather limited present data obtained at temperatures of 923 and 973 K should be considered with caution.

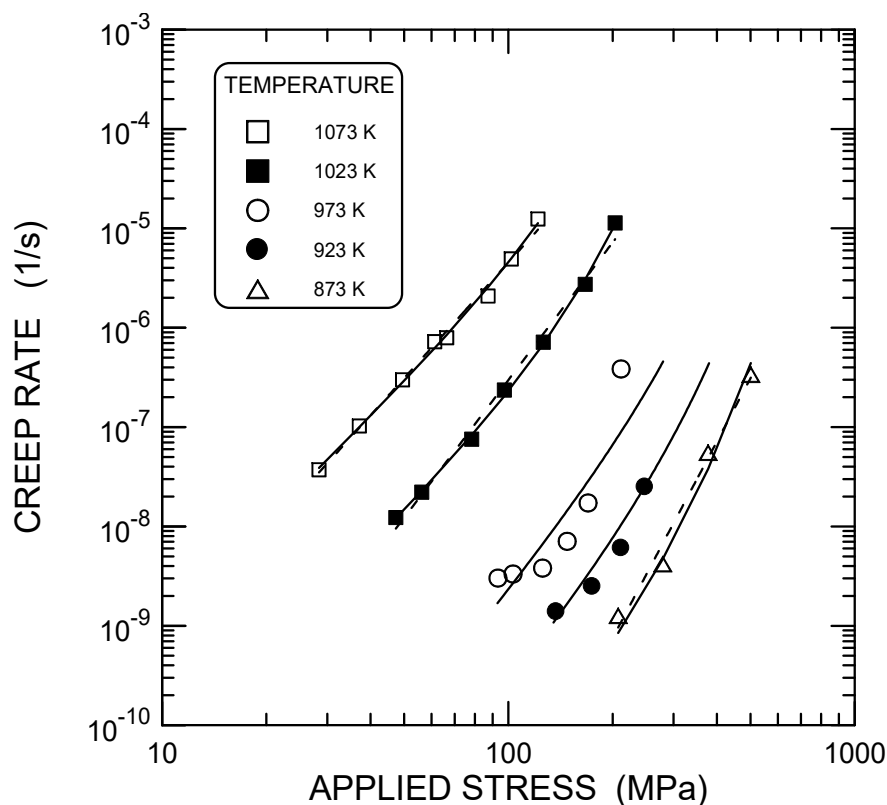


Figure 4. Dependence of the creep rate on applied stress. Solid lines: Garofalo Equation (3), dashed lines: power functions.

Table 1. Calculated values of parameters in Equation (3).

T [K]	A [1/s]	Q [kJ/mol]	B [1/MPa]	n
873–973	23.16	322.0	0.0045	4.23
1023–1073	48.38	544.6	0.0096	3.41

4. Discussion

The determination of the rate-controlling creep mechanism is usually based on a comparison of the measured value of power n with the theoretical models published in the literature. Models predict that $n = 1$ corresponds to diffusional creep, $n = 2$ to grain boundary sliding and n between 3 and 7 to dislocation

creep [26]. Values of the power of n , whether obtained directly from logarithmic dependencies or using Equation (3), indicate that creep is controlled by dislocation motion. The estimated activation energies at both high and low temperatures are higher than the activation enthalpy of the diffusion of iron in the B2 phase (270 kJ/mol [27], 234 kJ/mol [28]). The effective activation enthalpy for diffusion in a multicomponent alloy can be assessed by various approaches [29–31]. Their detailed discussion is beyond the scope of the present contribution. A weighted average of the enthalpies of the individual elements can be used as an approximate estimate of the effective activation enthalpy. The activation enthalpy of Co diffusion in B2 Fe–Co is 247 kJ/mol [32]. Problems associated with the availability of the isotope ^{26}Al lead to the recommendation of 214 kJ/mol as a suitable value for the activation enthalpy of aluminum diffusion in B2 [33]. The effective activation enthalpy then ranges from 232 to 250 kJ/mol. Even higher values of activation energy of creep (780 kJ/mol) can be determined over a temperature range from 973 K to 1023 K using the usual formula

$$Q = - \left[\frac{\partial \ln \dot{\epsilon}}{\partial (1/RT)} \right]_{\sigma} \quad (4)$$

The detected activation energies are, therefore, to be considered rather apparent values, resulting from the fact that neither the crystal lattice nor the microstructure are temperature-independent. As far as the crystal lattice is considered, the ternary phase diagram is known only for lower temperatures (see Figure 2). For higher temperatures, there is only an approximate estimate of the boundary between a single-phase and a two-phase structure [20]. At 1000 K, this boundary lies close to the chemical composition of the studied alloy. It is, therefore, likely that at 1023 and 1073 K, our alloy is single-phased and has a crystal lattice of type B2, or possibly, at the highest temperature, of type A2. Thus, a change from a single-phase to a two-phase structure and switching the crystal lattice from type B2 to an even more ordered type (an inverse-Heusler phase with possibly some disorder in some of the sublattices) when the temperature is reduced from the high-temperature to low-temperature region is likely to cause the high apparent activation energy of 780 kJ/mol. The more ordered inverse-Heusler phase is more resistant to deformation than a less-ordered B2 lattice or a disordered A2 lattice. Similarly, a two-phase structure is more resistant to deformation than a single-phase structure. Thus, changes in the creep rate as the temperature increases are not only due to the increase of the diffusion coefficient but also to the material weakening resulting from the changing microstructure and lattice disordering. Consequently, the apparent activation energy of creep is greater than the enthalpy of diffusion.

Figures 5 and 6 show a comparison of the stress dependence of the creep rate in the present alloy and a binary Fe-25 at. % alloy [34] at 873 K and 1073 K, respectively. The addition of cobalt significantly improves the creep resistance, particularly at the lower temperature. The comparison is complemented by the results of creep research in ternary alloys of Fe–Al–Ti, where the Heusler phase is also formed [16,35,36]. The data used for comparison were also obtained by the compressive testing. The data point of the alloy with 25 at. % Al and 20 at. % Ti at 873 K [35] was obtained by extrapolating the data at 1073 K using the appropriate activation energy and stress exponent. Evidently, at 1073 K, the effect of titanium additions on creep is somewhat more pronounced than the effect of cobalt addition. On the other hand, at a temperature of 873 K, the effects of the addition of both elements are approximately equal. This observation may be related to the position of both elements in the periodic table.

Recently, a ferritic alloy strengthened by coherent hierarchical precipitates has been developed [8,9]. Its excellent creep properties are due to the presence of Heusler-phase-based precipitates, which themselves contain coherent nano-scaled B2 zones.

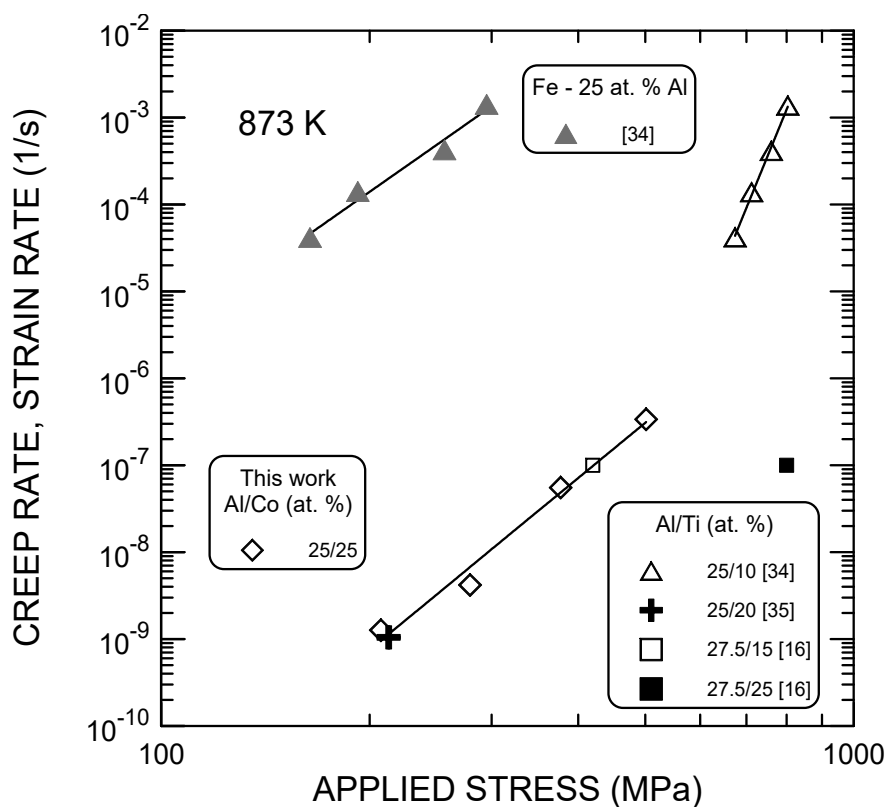


Figure 5. Comparison of creep rate/strain rate variation with applied stress for the present alloy, binary Fe–Al alloy and Fe–Al–Ti alloys at 873 K.

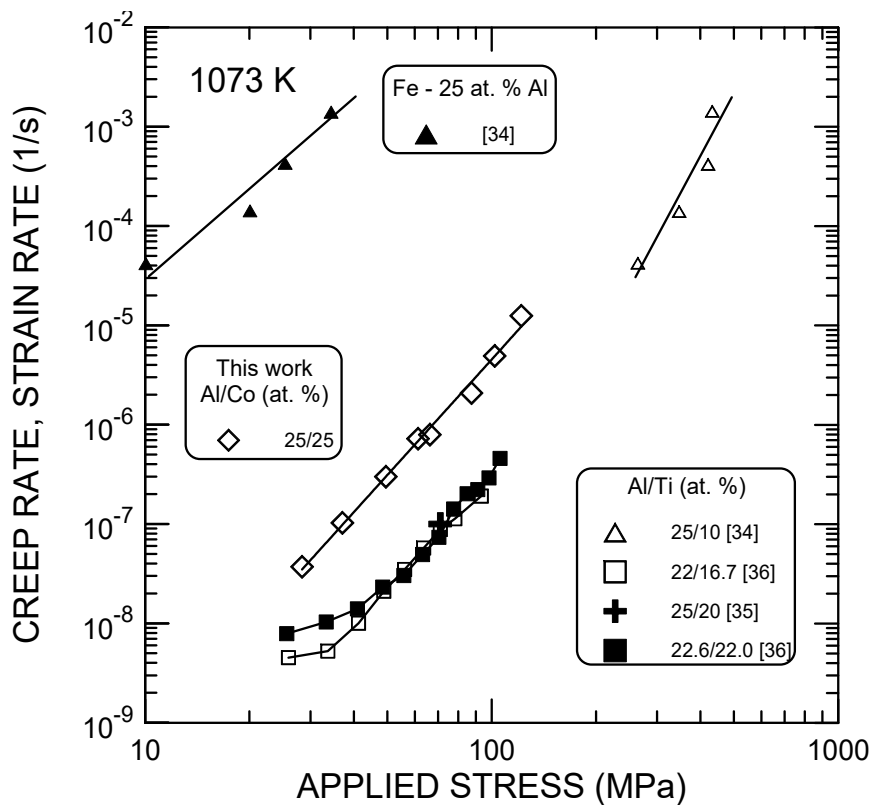


Figure 6. Comparison of creep rate/strain rate variation with applied stress for the present alloy, binary Fe–Al alloy and Fe–Al–Ti alloys at 1073 K.

Comparison of the creep data of this novel progressive alloy shows that the present laboratory alloy is slightly inferior as far as compressive testing at 973 K is concerned: Creep rates were $1.7 \times 10^{-8} \text{ s}^{-1}$ at 202 MPa and 1.5×10^{-7} at 220 MPa [8] vs. $1.7 \times 10^{-8} \text{ s}^{-1}$ at 170 MPa and $3.8 \times 10^{-7} \text{ s}^{-1}$ at 211 MPa (present alloy).

It is well-known that there are two non-equivalent positions for iron atoms in the Fe_3Al compound ordered into the L2_1 lattice: one with eight iron atoms as closest neighbors, the other with four iron atoms and four aluminum atoms as closest neighbors. The alloying elements to the left of Fe in the periodic table, such as Ti, preferentially occupy the former positions, whereas elements to the right of Fe (i.e., Co) occupy the latter positions [37,38]. The preference of positions has an influence on the stability of the L2_1 lattice. The addition of titanium leads to the stabilization, which results in an increase in the L2_1 –B2 transition temperature [39]. The situation in the inverse-Heusler lattice is more complicated (due to the existence of four sublattices) but the Co atoms are expected [19] to occupy the sublattice at locations where the second nearest neighbors are only the Fe and Co atoms (and not the Al atoms). It was also shown previously by quantum-mechanical calculations of Heusler-based Fe_2AlCo polymorphs, that the ordered full-Heusler structure is mechanically unstable and thermodynamically less stable than the inverse-Heusler lattice [13]. The energy differences between different polymorphs were found to be so small that partly disordered B2 and completely disordered A2 structures are predicted for elevated and high temperatures. The formation of polymorphs with disordered sublattices is thus probable with increasing temperatures similarly as phase-composition changes, i.e., a transition from a two-phase material to a single-phase one.

5. Conclusions

The creep of Fe-25 at. % Al-25 at. % Co alloy was studied in the temperature range from 873 K to 1073 K. The stress and temperature dependence of the creep rate was described by a combined Garofalo (sinh) and Arrhenius equation. The following conclusions regarding the creep resistance of the alloy can be drawn:

- The whole temperature range investigated can be divided into two regions with different values of the stress exponent and activation energy.
- The estimated activation energies at both high and low temperatures are higher than the effective activation enthalpy of diffusion resulting from the weighted average of enthalpies of individual components. An even greater value of the apparent activation energy was found in the transition between the two regions.
- The division into different regions can be explained by changes in the microstructure and crystal lattice ordering.
- The addition of cobalt significantly improves the creep resistance of the binary alloy Fe-25 at. % Al. However, at 1073 K, the effect of cobalt is less than that of titanium addition. At 873 K, the effects of both elements are comparable.

Author Contributions: Conceptualization: F.D.; Formal analysis: P.D.; Funding acquisition: M.F.; Methodology: F.D.; Resources: M.F.; Validation: F.D. and P.D.; Visualization: F.D. and M.F.; Writing—original draft: F.D.; Writing—review & editing: F.D., P.D. and M.F. All authors have read and agreed to the published version of the manuscript.

Funding: This research was funded by the Czech Science Foundation, grant number 17-22139S (F.D., P.D., M.F.).

Acknowledgments: Authors wish to thank Y. Jirásková (IPM Brno, Czech Republic) for the supply of the experimental alloys. This research has been financially supported by the Ministry of Education, Youth and Sports of the Czech Republic under the project m-IPMinfra (CZ.02.1.01/0.0/0.0/16_013/0001823) and under the project CEITEC 2020 (LQ1601). Figure 1 was visualized using the VESTA package [40].

Conflicts of Interest: The authors declare no conflict of interest.

References

1. Sauthoff, G. *Intermetallics*; VCH Verlagsgesellschaft: Weinheim, Germany, 1995; pp. 84–89. [[CrossRef](#)]
2. Stoloff, N.S. Iron aluminides: Present status and future prospects. *Mater. Sci. Eng. A* **1998**, *258*, 1–14. [[CrossRef](#)]
3. Liu, C.T.; George, E.P.; Maziasz, P.J.; Schneibel, J.H. Recent advances in B2 iron aluminide alloys: Deformation, fracture and alloy design. *Mater. Sci. Eng. A* **1998**, *258*, 84–98. [[CrossRef](#)]
4. Nathal, M.Y. Creep Deformation of B2 Aluminides. In *Ordered Intermetallics—Physical Metallurgy and Mechanical Behaviour*; Cahn, R.W., Sauthoff, G., Eds.; Kluwer Academic Publishers: Dordrecht, The Netherlands, 1992; pp. 541–563.
5. Nazmy, M.Y. Creep. In *Physical Metallurgy and Processing of Intermetallic Compounds*; Stoloff, N.S., Sika, V.K., Eds.; Chapman & Hall: New York, NY, USA, 1996; pp. 95–125.
6. Palm, M. Concepts derived from phase diagram studies for the strengthening of Fe–Al-based alloys. *Intermetallics* **2005**, *13*, 1286–1295. [[CrossRef](#)]
7. Morris, D.G.; Muñoz-Morris, M.A. Development of creep-resistant iron aluminides. *Mater. Sci. Eng. A* **2007**, *462*, 45–52. [[CrossRef](#)]
8. Song, G.; Sun, Z.; Li, L.; Xu, X.; Rawlings, M.; Liebscher, C.H.; Clausen, B.; Poplawsky, J.; Leonard, D.N.; Huang, S.; et al. Ferritic Alloys with Extreme Creep Resistance via Coherent Hierarchical Precipitates. *Sci. Rep.* **2015**, *5*, 16327. [[CrossRef](#)]
9. Song, G.; Sun, Z.; Clausen, B.; Liaw, P.K. Microstructural characteristics of a Ni₂TiAl-precipitate-strengthened ferritic alloy. *J. Alloy. Compd.* **2017**, *693*, 921–928. [[CrossRef](#)]
10. Gilleßen, M.; Dronskowski, R. A combinatorial study of inverse Heusler alloys by first-principles computational methods. *J. Comput. Chem.* **2010**, *31*, 612. [[CrossRef](#)]
11. Park, N.; Lee, S.-C.; Cha, P.-R. Effects of alloying elements on the stability and mechanical properties of Fe₃Al from first-principles calculations. *Comput. Mater. Sci.* **2018**, *146*, 303–309. [[CrossRef](#)]
12. Hasier, J.; Riolo, M.A.; Nash, P. Curie temperature determination via thermogravimetric and continuous wavelet transformation analysis. *EPJ Tech. Instrum.* **2017**, *4*, 5–16. [[CrossRef](#)]
13. Friák, M.; Oweisová, S.; Pavlu, J.; Holec, D.; Šob, M. An Ab Initio Study of Thermodynamic and Mechanical Stability of Heusler-Based Fe₂AlCo Polymorphs. *Materials* **2018**, *11*, 1543. [[CrossRef](#)]
14. Everhart, W.; Newkirk, J. Mechanical properties of Heusler alloys. *Heliyon* **2019**, *5*, e01578. [[CrossRef](#)] [[PubMed](#)]
15. Gorzel, A.; Palm, M.; Sauthoff, G. Constitution-based alloy selection for the screening of intermetallic Ti–Al–Fe alloys. *Z. Met.* **1999**, *90*, 64–70.
16. Prakash, U.; Sauthoff, G. Structure and properties of Fe–Al–Ti intermetallic alloys. *Intermetallics* **2001**, *9*, 107–112. [[CrossRef](#)]
17. Krein, R.; Friak, M.; Neugebauer, J.; Palm, M.; Heilmaier, M. L₂₁-ordered Fe–Al–Ti alloys. *Intermetallics* **2010**, *18*, 1360–1364. [[CrossRef](#)]
18. Garofalo, F. An empirical relation defining the stress dependence of minimum creep rate in metals. *Trans. Met. Soc. AIME* **1963**, *227*, 351–356.
19. Grover, A.K.; Pillay, R.G.; Nagarajan, V.; Tandon, P.N. Site preference and local environment effects in ferromagnetic ternary alloys. *J. Magn. Magn. Mater.* **1980**, *15*, 699–700. [[CrossRef](#)]
20. Kozakai, T.; Miyazaki, T. Experimental and theoretical studies on phase separations in the Fe–Al–Co ordering alloy system. *J. Mater. Sci.* **1994**, *29*, 652–659. [[CrossRef](#)]
21. Sellars, C.M.; McTegart, W.J. On the mechanism of hot deformation. *Acta Metall.* **1996**, *14*, 1136–1138. [[CrossRef](#)]
22. McQueen, H.J.; Cingara, A.; Ryan, N.D. New procedures for constitutive analysis (sinh-Arrhenius) and for flow curve calculation applied to 316 stainless steel. *Mater. High Temp.* **1992**, *10*, 201–206. [[CrossRef](#)]
23. Milička, K.; Dobeš, F. Constitutive description of creep behavior of M-4Al-1Ca alloy. *Strength Mater.* **2008**, *40*, 28–31. [[CrossRef](#)]
24. Castellanos, J.; Rieiro, I.; Carsí, M.; Ruano, O.A. Analysis of Garofalo equation parameters for an ultrahigh carbon steel. *J. Mater. Sci.* **2010**, *45*, 5522–5527. [[CrossRef](#)]
25. Dobeš, F.; Dymáček, P.; Hasegawa, M.; Iwashita, M. High-temperature creep of a CoNiCrAlY bond coat alloy. *Mater. Sci. Eng. A* **2019**, *759*, 272–277. [[CrossRef](#)]

26. Kassner, M.E.; Pérez-Prado, M.-T. Five-power-law creep in single phase metals and alloys. *Prog. Mater. Sci.* **2000**, *45*, 1–102. [[CrossRef](#)]
27. Tokei, Z.; Bernardini, J.; Gas, P.; Beke, D.L. Volume Diffusion of Iron in Fe₃Al: Influence of Ordering. *Acta Mater.* **1997**, *45*, 541–546. [[CrossRef](#)]
28. Mehrer, H.; Eggersmann, M.; Gude, A.; Salamon, M.; Sepiol, B. Diffusion in intermetallic phases of the Fe–Al and Fe–Si systems. *Mater. Sci. Eng. A* **1997**, *239*, 889–898. [[CrossRef](#)]
29. Darken, L.S. Diffusion, mobility and their interrelation through free energy in binary metallic systems. *Trans. AIME* **1948**, *175*, 184–201.
30. Fuentes-Samaniego, R.; Nix, W.D. Appropriate diffusion coefficients for describing creep processes in solid solution alloys. *Scr. Met.* **1981**, *15*, 15–20. [[CrossRef](#)]
31. Soliman, M.S.; El-Galali, I. Appropriate diffusion coefficients for dislocation creep in solid-solution alloys. *J. Mater. Sci. Lett.* **1998**, *7*, 1027–1030. [[CrossRef](#)]
32. Mehrer, H. Diffusion in intermetallics. *Mater. Trans. JIM* **1996**, *37*, 1259–1280. [[CrossRef](#)]
33. Eggersmann, M.; Mehrer, H. Diffusion in intermetallic phases of the Fe–Al system. *Philos. Mag. A* **2000**, *80*, 1219–1244. [[CrossRef](#)]
34. Zhu, S.-M.; Sakamoto, K.; Tamura, M.; Iwasaki, K. A comparative study of the high temperature deformation behavior of Fe–25Al and Fe–25Al–10Ti alloys. *Scr. Mater.* **2000**, *42*, 905–910. [[CrossRef](#)]
35. Krein, R.; Palm, M. The influence of Cr and B additions on the mechanical properties and oxidation behaviour of L21-ordered Fe–Al–Ti-based alloys at high temperatures. *Acta Mater.* **2008**, *56*, 2400–2405. [[CrossRef](#)]
36. Palm, M.; Sauthoff, G. Deformation behaviour and oxidation resistance of single-phase and two-phase L21-ordered Fe–Al–Ti alloys. *Intermetallics* **2004**, *12*, 1345–1359. [[CrossRef](#)]
37. Burch, T.J.; Litrenta, T.; Budnick, J.I. Hyperfine studies of site occupation in ternary systems. *Phys. Rev. Lett.* **1974**, *33*, 421–424. [[CrossRef](#)]
38. Nishino, Y.; Kumada, C.; Asano, S. Phase stability of Fe₃Al with addition of 3d transition element. *Scr. Mater.* **1997**, *36*, 461–466. [[CrossRef](#)]
39. Anthony, L.; Fultz, B. Effects of early transition metal solutes on the D0₃-B2 critical temperature of Fe₃Al. *Acta Met. Mater.* **1995**, *43*, 3885–3891. [[CrossRef](#)]
40. Momma, K.; Izumi, F. VESTA 3 for three-dimensional visualization of crystal, volumetric and morphology data. *J. Appl. Cryst.* **2011**, *44*, 1272. [[CrossRef](#)]



© 2020 by the authors. Licensee MDPI, Basel, Switzerland. This article is an open access article distributed under the terms and conditions of the Creative Commons Attribution (CC BY) license (<http://creativecommons.org/licenses/by/4.0/>).